MRS Communications (2022) 12:358–364

https://doi.org/10.1557/s43579-022-00185-6

MRS Communications

Research Letter

Polymer-BiI_3 composites for high-performance, room-temperature, direct X-ray detectors

Ritu Chaudhari and **Chhaya Ravi Kant**, Department of Applied Sciences and Humanities, Indira Gandhi Delhi Technical University for Women, Kashmere Gate, Delhi 110006, India
Alka Garg, Gargi College, University of Delhi, Siri Fort Road, New Delhi 110049, India
Address all correspondence to Chhaya Ravi Kant at **chhayaravikant@igdtuw.ac.in**

(Received 29 January 2022; accepted 5 April 2022; published online: 22 April 2022)

Abstract

Low-energy X-rays have a predominant role in medical diagnostic applications, grown tremendously during recent Covid-19 pandemic times. Synthesis of stable, PMMA/polystyrene-BiI_3 composites has been done through a facile, low-cost, dry-tumble mixing technique for direct X-ray detector applications. Comparative analysis of structural, optical, and photocurrent responses upon irradiation with low-energy X-rays (30 and 60 kV) ensue that PS-BiI_3 demonstrates high SNR 3300, sensitivity 189 μC Gy^{-1} cm^{-3} and fast response time 30 ms, at dose rate 1.68 mGy s^{-1}, affirming the composite to be prospective candidate for low-energy, room-temperature, direct X-ray detectors under low bias conditions.

Introduction

Low-energy, pulsed X-rays are being used in many medical diagnostic applications like digital radiography, dental X-ray imaging, CT scan, and radiation therapy. In recent times of COVID-19 pandemic, X-ray-based imaging devices have been widely used for chest scans rendering the CT score value, a vital parameter for an early detection of deteriorating lung condition that has helped doctors to give a timely treatment to the Covid-positive patients saving many lives.[1] These spectacular applications are appealing and have given a new surge in the research of X-ray detector materials. Although many semiconductor and perovskite materials have carved a niche in the commercial X-ray detector industry, still the X-ray interactions with the detector material pose challenges to obtain stable, high detector performance with repeated usage. Researchers need to envisage new generation, light weight, portable, economically viable, easy-to-synthesize, X-ray detector materials possessing mechanical flexibility and capability of room-temperature operations with low power requirements. In this paper, we have synthesized polymer-BiI_3 composite pellets using a facile, soft effective method and investigated their performance for potential usage in direct X-ray detectors, capable of operating at room temperature, under low bias conditions.

X-ray detectors are broadly classified on two operation mechanisms, direct and indirect. Traditional semiconductor detectors are based on direct x-ray detection mechanism wherein the incident X-rays radiations are absorbed by the detector material and directly converted to charge carriers, generating an electric signal unlike the indirect detectors where the incident radiations fall on a scintillator material producing scintillating photons which further generate an electric signal. Direct X-ray detectors possess better signal-to-noise ratio (SNR) and sensitivity and establish a stronger presence in the market. Compound semiconductors with wide bandgap show capability of room-temperature operations, notwithstanding the crystal defects and charge trapping that lead to performance deterioration. Direct conversion radiation detector materials should possess the following: (1) high density and high atomic number, since absorption coefficient (α) is proportional to Z^4/E^3, where Z and E denote the atomic number of material and radiation energy, respectively; (2) high μτ, product of charge carrier mobility, and lifetime for efficient charge collection; (3) high resistivity to suppress the noise current; and (4) good stability for long-term operation.[2]

α-Se is the most prevalent direct conversion material used commercially in X-ray imaging devices, but poses certain limitations such as requirement of high operational voltage (10,000 V mm^{-1}) and decrease in the attenuation coefficient beyond X-ray energies of 40 keV.[3] Gallium arsenide being robust and stable makes a strong choice for imaging detectors; however, it shows poor energy resolution.[4] Cd-based detector materials such as cadmium telluride and cadmium zinc telluride exhibit good energy resolution and higher detection efficiency at high x-ray energies, but the main challenges with these materials are inconsistent performance at high x-ray flux, lower sensitivity, and high toxicity.[5] Recently, perovskite-based metal halides[6–9] like $MAPbI_3$ (methyl ammonium lead iodide) and $Cs_2AgBiBr_6$ (dicesium silver bismuth hexabromide) are also emerging as potential candidates for modern detectors as they successfully demonstrate low dark current, high sensitivity at low energy doses, and a stable output over prolonged long usage.[10, 10] They display a linear response to X-ray energy and applied bias; however, high defect density, ion migration at high voltages, and poor environmental stability are a hindrance

in their practical applications. $Cs_3Bi_2I_9$ is an excellent choice for x-ray detector due to its high sensitivity, low detection limit, dose rate linearity, and incredible detector properties;[12, 13] nevertheless, the detector performance parameters are highly dependent on the controlled synthesis method which is an expensive and sophisticated. Reliability and reproducibility of results with environmental stability are major challenge for these detectors in practical applications. Challenge still remains to find an economical, sturdy, non-toxic, and easy-to-synthesize material which demonstrates high-performance detector metrics.[14, 15]

In the past, bismuth tri-iodide (BiI_3), a high density (5.78 g cm^{-3}), high atomic number (Bi:83, I:53) material offering high resistivity (10^8 to 10^{13} Ω-cm) and high attenuation, has shown magnificent results for lead-free, X-ray and gamma-ray detection applications.[16, 17] However, BiI_3 has poor environmental stability and has a difficult growth process for defect free thick samples. In order to mitigate these shortcomings, we have, in our previous work, reported synthesis and preliminary investigations on polystyrene (PS)-BiI_3 composites and our results were indicative of good stability and prospects of the new composite for radiation detector.[18] The polymer matrix reinforces a level of stiffness in the otherwise easily cleavable layered pristine BiI_3 and further increases the overall resistivity of the resultant composite thereby augmenting its performance parameters with remarkable improvement in detector stability. These results were encouraging and actuated us to carry out more studies on polymer-BiI_3 composites.

In the current work, we have synthesized and investigated the properties of poly-methyl methacrylate (PMMA)-BiI_3 and polystyrene (PS)-BiI_3 composites for being a radiation detector material and further compared its prospects vis a PS-BiI_3 samples. Photocurrent response of these composite pellets has been investigated with X-ray irradiation from two pulsed X-ray sources (60 kV and 30 kV) used in practical dental applications. PMMA-BiI_3 composite pellets showed sensitivity and SNR as 94.6 μC mGy^{-1} cm^{-3} and 1360, respectively, for dose rate of 1.68 mGy s^{-1} at 100 V and 7.99 μC Gy^{-1} cm^{-3} and 495, respectively, at dose rate of 5.33 mGy s^{-1} at voltage of 1.5 V. PS-BiI_3 composite showed better sensitivity and SNR values of 189 μC Gy^{-1} cm^{-3} and SNR 2300 for dose rate of 1.68 mGy s^{-1} for irradiation with X-ray energy of 30 kV. A considerable improvement to 3300 SNR was achieved with increase in dose rate to 5.33 mGy s^{-1} at 1.5 Volts though at a slightly compromised sensitivity of 3.48 μC Gy^{-1} cm^{-3}. It should be noted that this dose rate is the lowest for the X-ray source in our facility used for this work. As stated by the definition of the International Union of Pure and Applied Chemistry (IUPAC), detection limit of the device defined as the dose rate yielding an SNR value of 3 at a fixed bias which signifies that for prepared detector the actual detection rate is less than this value.[11] The photocurrent results demonstrated by polymer-BiI_3 composites suggest them to be prospective material for X-ray detection, offering good SNR response in the dose rate of 3–5 μGy s^{-1} at low voltage of 1.5 V as (most X-ray diagnostics for medical applications are done below 5 mSv or 5.5 μGy s^{-1}[19]). Generally, such high SNR values are achieved at high bias voltage of the order of hundred voltage which reduces the stability of the detector. However, in our studies, we have successfully achieved high SNR at low voltage of 1.5 V.

Materials and methods

Synthesis of polymer-BiI_3 composite pellets

BiI_3 (purity > 99.9%), PMMA , and PS granules were purchased from Sigma-Aldrich and polymer-BiI_3 composites were synthesized by simple dry-tumble technique with hot compression method. PMMA and PS granules were ground separately to fine powder in a liquid nitrogen environment using a grinder. Homogeneous composites were prepared by dry mixing the micron-sized crushed polymer powder with same-sized BiI_3 powder at different weight percentage ratio of PMMA:BiI_3 (70:30, 60:40, 50:50, 40:60) and PS: BiI_3 (50:50) and the nomenclature of the samples has been adopted accordingly as shown in Table I. The dry mixing was done without any solvent with constant stirring on a magnetic stirrer for 1 h at 400–500 rpm speed at room temperature. The solvent-free method prevents traces of any impurities due to no solvent residue left in the composite. The composite mixture was put into a stainless-steel dye in a hot compression press and slowly heated to temperatures just below the softening temperature of the polymer 120 °C and 95 °C for PMMA and PS, respectively, maintaining the temperature for 15 min to achieve uniform heating and mixing of the composite powder. The mixture was then pressed with a pressure of 50–60 kg cm^{-2} to form a 1.2–1.5 mm thick compact pellet and let the composite gradually cool down to room temperature. The gradual heating and cooling process assists in the synthesis of a uniform and homogeneous composite with better crystallinity (Fig. 4 supplementary data). The as-prepared $20 \times 10 \times 1.5$ mm^3 pellets were cut into different rectangular dimensions for further characterization.

Characterization and measurements

The X-ray diffraction studies of the samples were done using CuKα1 radiation in the 2θ range of 10°–50°. The optical studies of the samples were done using Double

Table I. Nomenclature of samples according to weight % composition of PMMA, PS, and BiI_3.

Sample name	BiI_3 wt%	Polymer wt%
PMMA-70	30%	PMMA 70%
PMMA-60	40%	PMMA 60%
PMMA-50	50%	PMMA 50%
PMMA-40	60%	PMMA 40%
PS-50	50%	PS 50%

Beam Cary 100 UV–Vis spectrometer within the spectral range of 200–800 nm. The morphology of the surface as well as cross-sectional and top view across the thickness of the pellet have been performed by ICM-7000 Jeol Scanning Electrode Microscope with an EDAX. To study the X-ray detection response, the composite pellets were placed at 15 cm from the X-ray source and were irradiated using two different pulsed, DC X-ray sources operating at 30 kV (tube current 10 mA, pulse width 4 s, 1.68 mGy s^{-1} dose rate) and 60 kV (tube current 8 mA, pulse width 1.5 s, dose rate of 5.33 mGy s^{-1}) in on/off states. The X-rays are made to exit from the source through 1.5 mm thick Al foil filters. The dose rate (D) for the source is calculated by formula (1) in supplementary data.

The photocurrent measurements were done using an Keithley-6485 Picometer with silver electrodes deposited on the 1.5 mm thick detectors in perpendicular configuration. The interaction of X-rays with detector material strongly depends on the stopping power or the attenuation coefficient of the material. The mass attenuation coefficient of the composite at a particular energy was calculated by NistXcom software (https://physics.nist.gov/PhysRefData/Xcom/html/xcom1.html) and was multiplied by the weighted average density of the composite to obtain linear attenuation coefficient of the material. The absorbance/attenuation of radiation as calculated from Eq. (2) in supplementary was upto 95% for our samples.

Results and discussion

UV spectroscopy, X-ray diffraction and SEM studies

The UV absorption spectra of the samples PMMA-40 and PMMA-70 as depicted in Fig. 1(a) were recorded after dissolving the pellet in acetone solvent. The polymer PMMA functional OH-group formed bond with Iodine (I) in BiI_3 in solid pellet matrix but when we dissolve the pellet in solvent, the OH-I bond weakened and got two different peaks.[20] These two are very similar to the pristine BiI_3 absorption peaks (Fig. 2 supplementary data) with a blue shift that indicates the formation of composite. The spectra show onset of absorption in the range of 450–480 nm with a broad peak and another sharp transition edge at 350 nm which progresses to peak at 330 nm. There is an I-OH bond formation in our composite samples. An increase in BiI_3 weight percentage from 30 to 60% leads to a decreased concentration of I–OH bonding. This leads to changes in the nature of intermolecular bands within the spectrum which may act as defect or trap states thereby leading to the difference in the onset of absorption leading to the peak shift. The bandgap for the PMMA-BiI_3 composites as calculated from Tau plot [inset in Fig. 1(a)] is 2.44 eV which lies between the bandgap values of its constituents (BiI_3, 2.0 eV, and PMMA, 4.8 eV) and is also the desired bandgap for X-ray detector materials. An increase in the concentration of PMMA from 40 to 70% leads to a substantial increase in the absorption peak intensity at 390 nm and furthermore, the onset of

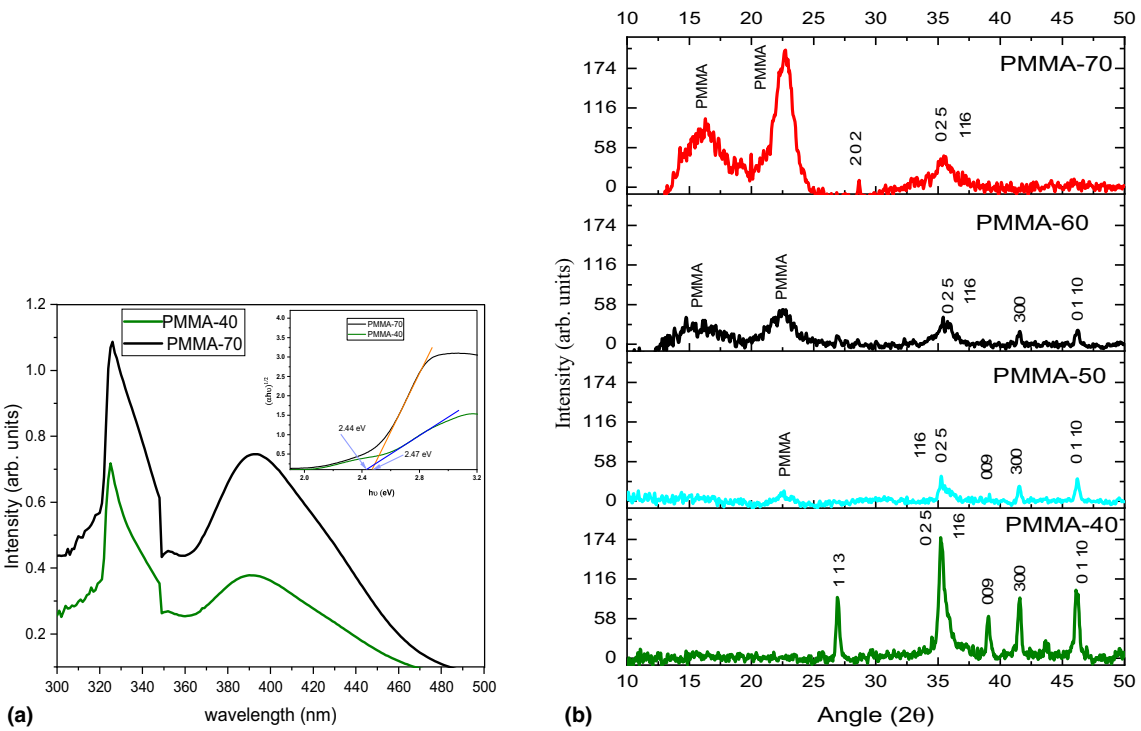

Figure 1. (a) UV–Vis absorption spectra of PMMA-70 and PMMA-40 samples, inset: tauc plot for band gap (b) XRD pattern of polymer-BiI_3 composites at varied ratios for PMMA-40,50,60,70.

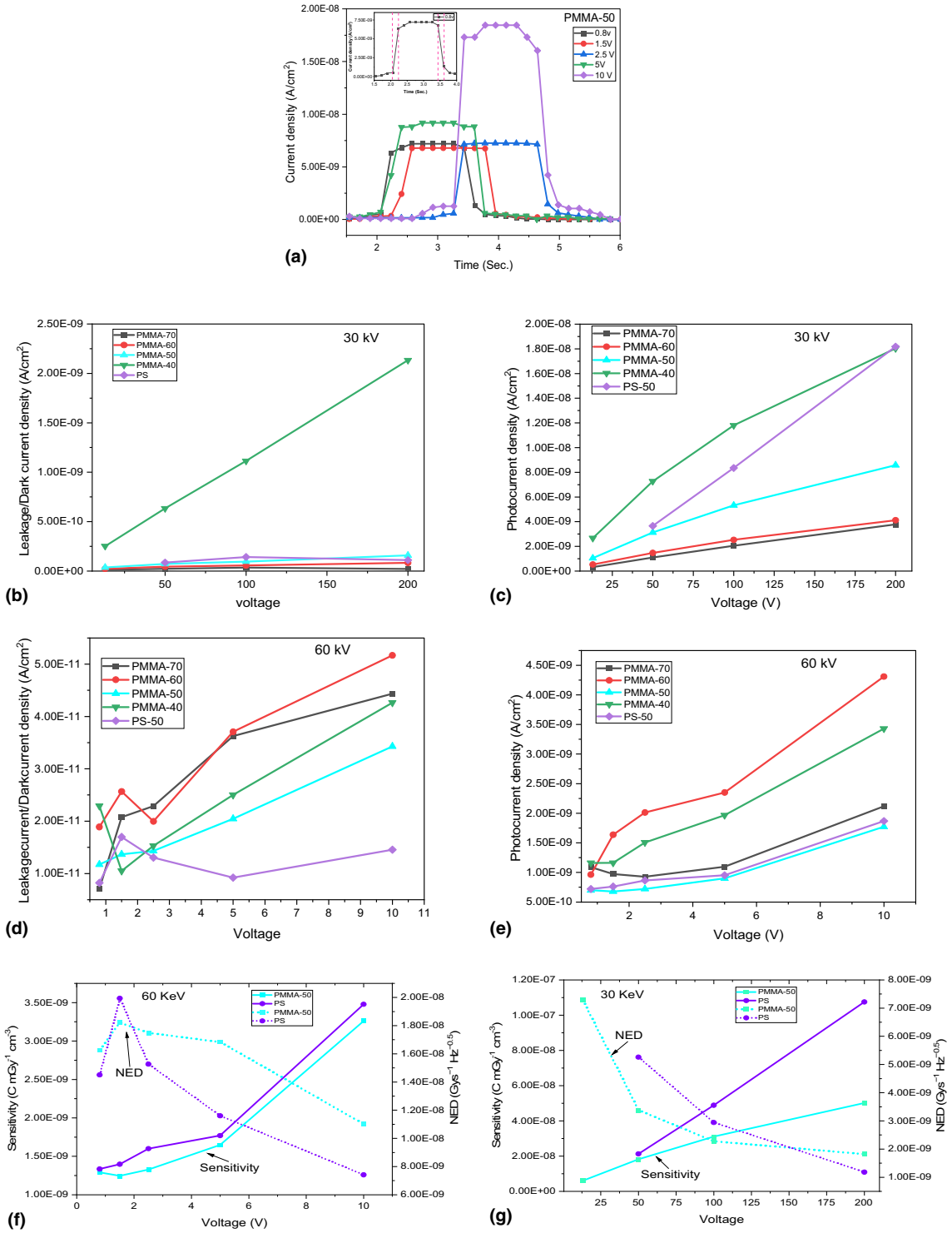

Figure 2. Photocurrent studies for PMMA and PS composite samples for X-ray irradiation at 60 kV and 30 kV. (a) Photocurrent versus time response (inset depicts the rise and fall time of the response curve for PMMA-50), (b, c, d, and e) Leakage current density and photocurrent density versus bias voltage for polymer-BiI3 composites. (f, g) Sensitivity and NED response of best results PMMA-50 and PS-50 samples at 60 kV and 30 kV, respectively (solid lines represent sensitivity and dotted lines represent NED).

absorption gets slight red shifted from 470 to 480 nm. The broad band from 350 to 480 nm may be attributed to the presence of defects, color-centeres, and vacancies leading to trapping of electrons and holes.[21]

X-ray diffraction patterns of the composite samples synthesized with varied compositional ratios depicted in Fig. 1(b) show multiple peaks corresponding to PMMA and BiI_3. Pure PMMA gives two broad peaks at around 14° and 21.6°, which is seen shifted at around 15.5° and 22.5° in our samples, suggestive of compressive stress induced during the composite formation.[22] The peak at around 35.1° is a merged peak of (025) and (202) BiI_3 planes and is clearly evident as a shoulder in the pattern for PMMA-70. This peak along with (300) peak corresponds to the tetragonal phase with space group P3/m of BiI_3 (compared with JPCDS card no. #76-1742). Further, the (0110) and (009) peaks represent hexagonal phase of BiI_3 asserting mixed phases in our samples (JPCDS card no. #48-1795). It is worth mentioning here that with increasing polymer content, the BiI_3 peaks diminish and there is a gradual progression toward amorphous nature in the composite formation. The PMMA-50, 60 patterns expose well-defined crystalline peaks for both PMMA and BiI_3 evincing the fact that BiI_3 crystallites are homogeneously embedded near the surface in the PMMA matrix. These samples pre-eminently show well-balanced properties of both BiI_3 and PMMA, ensuing better charge collection efficiency for a wider range of voltages as can be corroborated with our results later.

The surface morphology of the PMMA-50 sample given in Fig. 3 (supplementary data) showed a homogeneous composite with a sheet structure rolled in at the edges corresponding of PMMA with small BiI_3 crystallites sparsely spread all over the surface of the sheet and at the boundaries of the folds. Cross-sectional micrograph gives the average thickness of the sample as 1.5 mm. The energy-dispersive X-ray analysis of the sample portion marked in red as SPC001showed the presence of bismuth and iodine peaks thereby corroborating our XRD results. Further, SEM study of the sample revealed no structural changes after continuous sun exposure of the sample for over 60 min, and more so no impairment in the features was found even after being kept under high humidity (RH 70–90%) and high temperature (30–35°C) conditions for 2 months asserting the environmental stability of the samples. EDAX studies confine homogenous composite across sample and its cross-section (Fig. 4 in supplementary data).

Photocurrent and performance metrics analysis

We have investigated the detector performance parameters like photocurrent, leakage/dark current, SNR, sensitivity, and noise-equivalent dose (NED) for PMMA-BiI_3 and PS-BiI_3 composites synthesized with different ratios. However, analysis of PS composite results conclusively declared PS-50 to be the best sample in terms of low leakage current, high photocurrent, and high SNR. Therefore, to maintain brevity of the manuscript, comparative results for PMMA composites vis a vis PS-50 have been cited. The photocurrent and dark-current responses upon irradiation with two different X-ray sources (60 kV, 8 mA) and (30 kV, 10 mA) at different bias voltages are depicted in Fig. 2(a–f). Photocurrent time response of PMMA-50 sample shows a sharp rise and fall with switching on/off of the X-ray source in Fig. 2(a) [photo-response for 30 kV of PMMA-50 sample is included in supplementary data Fig. 5(b)] and calculations yield a fast response time of around 30 ms (inset Fig. 2a). Fast response/recovery time is highly desired in medical applications for improved image resolution and reduced X-ray exposure. A point worth mentioning here as an advantage of our results is the requirement of low bias voltage (1–10 V) to achieve substantial photocurrent values at X-ray energy, 60 kV. High bias conditions adversely affect the photocurrent signal due to polarization effects induced in the sample. Figure 2(b–e) displays a nearly linear response between the photocurrent and dark-current signals versus bias voltage in our samples and further reveals reduction in the signals by an order of 1 to 2 with increase in X-ray energy from 30 to 60 kV. For an ideal detector, high photocurrent and low leakage current are key parameters to appraise the detector performance, and PMMA-40 and PMMA-60 samples demonstrated a high photocurrent, but on the flipside showed unfavorably high leakage current. PMMA-50 exhibited minimum leakage-current density, 1.17×10^{-11} A cm^{-2} (at 0.8 V, 60 kV) and 3.68×10^{-11} A cm^{-2} (at 13 V, 30 kV) bias voltage. The photocurrent signals recorded for PMMA-50 was of the order of 7×10^{-10} A cm^{-2} (at 0.8 V, 60 kV) and 3.13×10^{-09} A cm^{-2} (at 50 V, 30 kV). Although PMMA-50 offers low photocurrent densities, smaller standard deviation, low leakage current, and better SNR that are reasonable trade-off in detector performance parameters, consequently making PMMA-50, the optimal sample in the PMMA series. However, comparison between PMMA-50 and PS-50 rendered better results for the latter, with PS-50 displaying lower leakage current, 8.21×10^{-12} A cm^{-2} (at 0.8 V, 60 kV) and comparable photocurrent densities, 7.2×10^{-10} A cm^{-2} (at 0.8 V, 60 kV) and 3.66×10^{-09} A cm^{-2} (at 50 V, 30 kV). High photocurrent and low leakage currents offered by PS-50 make it a prospective choice for the detector. PS-50 photocurrent response for 60 kV is given in supplementary data (Fig. 5). Signal-to-noise ratio (SNR), sensitivity, and noise-equivalent dose rate (NED) are crucial assessment parameters for a detector and are calculated with formulas given in supplementary data.

A detector should possess a low NED value for better quality, high contrast imaging, which is an important parameter for practical medical applications.[21] Calculations for sensitivity, SNR, and NED have been done for dose rates, (D) of 5.33 mGy s^{-1} (60 keV source) and 1.68 mGy s^{-1} (30 kV source). Highest achieved sensitivity and SNR for different dose rates and bias conditions by PMMA composites in our work are mentioned in sequence as follows: (94.6 μC mGy^{-1} cm^{-3}, 1360 for dose rate 1.68 mGy s^{-1}, at 100 V) and (7.99 μC Gy^{-1} cm^{-3}, 495, for dose rate of 5.33 mGy s^{-1}, at 1.5 V). PS-50 composites showed best sensitivity and SNR values as (189 μC Gy^{-1} cm^{-3}, 2300 for dose rate of 1.68 mGy

Table II. Comparison of sensitivity results for PMMA and PS composites in this work with other published data.

Material	Sensitivity (μC Gy^{-1} cm^{-3})	X-ray tube voltage (kV)	Dose rate (mGy s^{-1})	Voltage/electric field	Ref.
$CsPbI_3$: PVDF-HFP	4.7	70	2.5	2 V	[24]
BiI_3	0.053	70	2.5	2 V	[25]
Bi_5O_7I	1.926	70	2.5	2 V	[26]
TMCM-$CdCl_3$	128.9±4.64 μC Gy^{-1} cm^{-2}	40	1.06 μGy^{-1} s^{-1}	10 V	[27]
ω-Bi_2O_3	3.077 μCGy^{-1} cm^{-2}	60	56.95 μGy^{-1} s^{-1}	20 V	[28]
$CsPbI_3$	83.6 μC Gy^{-1} cm^{-2}	60	1.7	0.17 V $μm^{-1}$	[29]
Y_2O_3 (high temp.)	0.143	70	2.5	2 V	[30]
Fe doped β-Ga_2O_3	23.2 nC Gy^{-1}	30	0.383 Gy s^{-1}	800 V	[23]
PMMA-BiI_3	94.6	30	1.68	200 V	This work
PMMA-BiI_3	7.99	60	5.33	10 V	This work
PS-BiI_3	189	30	1.68	200 V	This work
PS-BiI_3	3.48	60	5.33	10 V	This work

s^{-1}, at 100 V) and (3.48 μC Gy^{-1} cm^{-3}, 3300, for dose rate of 5.33 mGy s^{-1}, at 1.5 V) indicating an exceptionally high SNR of 3300, though at a slightly compromised sensitivity of 3.48 μC Gy^{-1} cm^{-3}. The highest sensitivity accomplished in our work surpasses that of commercially available α-Se detectors, which is 20 μGy^{-1} cm^{-2} at 10,000 V. Sensitivity and NED values for PMMA-50 and PS-50 are (3.26 μGy^{-1} cm^{-3}, 1.10×10^{-8} Gys^{-1} $Hz^{-0.5}$) and (3.48 μGy^{-1} cm^{-3}, 7.42×10^{-9} Gys^{-1} $Hz^{-0.5}$), respectively, The sensitivity in our samples is much higher than the reported relative sensitivity value of 23.2 μC Gys^{-1} for β-Ga_2O_3 MSM detector at 800 V bias voltage and also better than the value, 21.8 nC Gy^{-1}, reported for β-Ga_2O_3 SBD detector at 10 V. Enumerating further, the NED values of PMMA-50 and PS-50 samples are lower by an order of 2 and outperform the reported NED values for β-Ga_2O_3 MSM detector (4.13×10^{-7} Gys^{-1} $Hz^{-0.5}$) and β-Ga_2O_3 SBD detector (8.69×10^{-7} Gys^{-1} $Hz^{-0.5}$).[23] A comparative table with sensitivity values for our samples vis a vis those reported in recent literature reports is given in Table II.

High SNR, better sensitivity, and low NED, more so at low bias conditions, all together make polymer-BiI_3 composites, the preferred choice for high imaging X-ray detectors in medical diagnostics. PS composites that have an edge over PMMA composites exhibiting better response for 60 kV X-ray source such as high sensitivity, SNR, low dark current, and NED for response. On the contrary, PMMAcomposite with a higher mass attenuation for low energies showed faster rise and fall response at low voltages. Further, the standard deviation of photocurrent of optimized composite samples was found 0.21% for PMMA-50 and 0.02% for PS, which is way less than the standard value (10%). PS-BiI_3 samples proved to be more environmentally stable with longer operational life as the OH^- group in the PMMA samples causes rusting under ambient and humid conditions arising the need for surface cleaning before doing photocurrent measurements. Also, these polymers being thermostatic can be reused over repeated cycles with reliability which is a problem with halide-based detectors.

Conclusion

To conclude, a low-cost solvent-free method has been used to prepare lead-free, PMMA/PS- BiI_3 composite pellets of thickness 1.5 mm, which displays attenuation upto 95% of incident X-rays. Both polymer composites showed promising results for room-temperature X-ray detector operation under low bias conditions with good environmental stability. But among both, PS-50 showed outstanding results of x-ray response for both 30 and 60 kV X-rays with better environmental stability. The sensitivity achieved for PS-50 was 189 μC Gy^{-1} cm^{-3} which is nine times better than the commercially available α-Se (20 μC Gy^{-1} cm^{-2}). Also, the SNR, 3300 demonstrated by the PS-50 composite at 1.5 V biased voltage holds great promise for fabrication of a good X-ray imaging device with high resolution at low bias voltages. The response and recovery time of the detector is fast around 30 ms. The reliability of these materials is high owing to smaller standard deviation in photocurrent as well as noise current measurements. These results suggest that the PMMA/PS -BiI_3 composites, exhibiting fabulous properties, are a fantastic candidate for room-temperature, low-voltage, radiation detector devices. Yet, sensitivity of the sample further needs to be improved, which can be achieved by using conductive fillers to increase the photocurrent.

Acknowledgments

The authors would like to acknowledge Dr. Kulvinder Singh, Deen Dayal Upadhyaya College, University of Delhi, for allowing use of X-ray facility in his lab and further acknowledge Dr. Akhilesh Pandey, Scientist F SSPL, DRDO, for his support to do XRD characterization of our samples. The authors are thankful to Indira Gandhi Delhi Technical University for Women for the lab infrastructure and research facilities and also Ritu Chaudhari is thankful to IGDTUW for financial support through Junior Research Fellowship. The authors also thank to reviewers for their valuable feedbacks.

Declarations

Conflict of interest

The authors have no conflict of interests relevant to this article.

Supplementary Information

The online version contains supplementary material available at https://doi.org/10.1557/s43579-022-00185-6.

References

1. A. Vaiserman, A. Koliada, O. Zabuga, Y. Socol, Health impacts of low-dose ionizing radiation: current scientific debates and regulatory issues. Dose-Response **16**(3), 1–27 (2018). https://doi.org/10.1177/1559325818796331
2. G.W. Grodstein, X-ray attenuation coefficients from 10 key to 100 Mev. US Dep. Commer. Natl. Bur. Stand. **1**, 58 (1957)
3. H. Huang, S. Abbaszadeh, Recent developments of amorphous selenium-based X-ray detectors: a review. IEEE Sens. J. **20**(4), 1694–1704 (2020). https://doi.org/10.1109/JSEN.2019.2950319
4. P.J. Sellin, Recent advances in compound semiconductor radiation detectors. Nucl. Instrum. Methods Phys. Res. A **513**(1–2), 332–339 (2003). https://doi.org/10.1016/j.nima.2003.08.058
5. C. Szeles, CdZnTe and CdTe materials for X-ray and gamma ray radiation detector applications. Phys. Status Solidi **241**(3), 783–790 (2004). https://doi.org/10.1002/pssb.200304296
6. Y. Liu et al., Inch-size 0D-structured lead-free perovskite single crystals for highly sensitive stable X-ray imaging. Matter **3**(1), 180–196 (2020). https://doi.org/10.1016/j.matt.2020.04.017
7. M. Hu et al., Large and dense organic-inorganic hybrid perovskite $CH_3NH_3PbI_3$ wafer fabricated by one-step reactive direct wafer production with high x-ray sensitivity. ACS Appl. Mater. Interfaces **12**(14), 16592–16600 (2020). https://doi.org/10.1021/acsami.9b23158
8. X. Zheng et al., Ultrasensitive and stable X-ray detection using zero-dimensional lead-free perovskites. J. Energy Chem. **49**, 299–306 (2020). https://doi.org/10.1016/j.jechem.2020.02.049
9. Y. Liu et al., Large lead-free perovskite single crystal for high-performance coplanar X-ray imaging applications. Adv. Opt. Mater. **8**(19), 1–12 (2020). https://doi.org/10.1002/adom.202000814
10. H. Zhang et al., High-sensitivity X-ray detectors based on solution-grown caesium lead bromide single crystals. J. Mater. Chem. C **8**(4), 1248–1256 (2020). https://doi.org/10.1039/c9tc05490a
11. W. Pan et al., $Cs_2AgBiBr_6$ single-crystal X-ray detectors with a low detection limit. Nat. Photon **11**(11), 726–732 (2017). https://doi.org/10.1038/s41566-017-0012-4
12. A. Datta, Z. Zhong, S. Motakef, A new generation of direct X-ray detectors for medical and synchrotron imaging applications. Sci. Rep. **10**(1), 1–10 (2020). https://doi.org/10.1038/s41598-020-76647-5
13. Y. Zhang et al., Nucleation-controlled growth of superior lead-free perovskite $Cs_3Bi_2I_9$ single-crystals for high-performance X-ray detection. Nat. Commun. **11**(1), 1–11 (2020). https://doi.org/10.1038/s41467-020-16034-w
14. T.C. Sum, S. Mhaisalkar, N. Mathews, Limitations of $Cs_3Bi_2I_9$ as lead-free photovoltaic absorber materials. ACS Appl. Mater. Interfaces (2018). https://doi.org/10.1021/acsami.7b14735
15. X. Zhou et al., Lead-free perovskite single crystals: a brief review. Curr. Comput.-Aided Drug Des. **11**(11), 1–14 (2021). https://doi.org/10.3390/cryst11111329
16. M. Matsumoto, K. Hitomi, T. Shoji, Y. Hiratate, Bismuth tri-iodide crystal for nuclear radiation detectors. IEEE Trans. Nucl. Sci. **49**(5), 2517–2520 (2002). https://doi.org/10.1109/TNS.2002.803883
17. A.T. Lintereur, W. Qiu, J.C. Nino, J.E. Baciak, Iodine based compound semiconductors for room temperature gamma-ray spectroscopy. Opt. Photon. Glob. Homel. Secur. IV **6945**, 694503 (2008). https://doi.org/10.1117/12.777402
18. R. Chaudhari, A. Garg, K. Singh, M. Tomar, V. Gupta, C. RaviKant, Bismuth tri-iodide-polystyrene composite for X-rays switching applications at room temperature. Radiat. Phys. Chem. **186**, 109538 (2021). https://doi.org/10.1016/j.radphyschem.2021.109538
19. D.R. Shearer, M. Bopaiah, Dose rate limitations of integrating survey meters for diagnostic X-ray surveys. Health Phys. **79**, S20–S21 (2000). https://doi.org/10.1097/00004032-200008001-00007
20. E. Wlaźlak, W. Macyk, W. Nitek, K. Szaciowski, Influence of π-Iodide intermolecular interactions on electronic properties of Tin(IV) iodide semiconducting complexes. Inorg. Chem. **55**(12), 5935–5945 (2016). https://doi.org/10.1021/acs.inorgchem.6b00336
21. K. Kumar, P. Arun, C. Ravi Kant, B.K. Juluri, Metal cluster's effect on the optical properties of cesium bromide thin films. Appl. Phys. Lett. **100**(24), 243106 (2012). https://doi.org/10.1063/1.4729061
22. R. Kumar, S.A. Ali, P. Singh, U. De, H.S. Virk, R. Prasad, Physical and chemical response of 145 MeV Ne6+ ion irradiated polymethylmethacrylate (PMMA) polymer. Nucl. Instrum. Methods Phys. Res. B **269**(14), 1755–1759 (2011). https://doi.org/10.1016/j.nimb.2010.12.025
23. L. Zhou et al., Pulsed x-ray detector based on Fe doped β-Ga_2O_3single crystal. J. Phys. D (2021). https://doi.org/10.1088/1361-6463/abf53b
24. R.R. Karthieka, G.D. Venkatasubbu, T. Prakash, Nanocomposite thick films of CsPbI3: PVDF-HFP on plastics for direct conversion low-dose X-ray sensor. Mater. Sci. Semicond. Process. **120**, 105289 (2020). https://doi.org/10.1016/j.mssp.2020.105289
25. R.R. Karthieka, R.N. Begum, T. Prakash, Direct conversion X-ray sensing nature of bismuth (III) iodide thick films. Chin. J. Phys. **71**, 643–650 (2021). https://doi.org/10.1016/j.cjph.2021.02.017
26. P. Praveenkumar, G.D. Venkatasubbu, P. Thangadurai, T. Prakash, Nanocrystalline bismuth oxyiodides thick films for X-ray detector. Mater. Sci. Semicond. Process. **104**, 104686 (2019). https://doi.org/10.1016/j.mssp.2019.104686
27. C. Ma et al., Centimeter-sized molecular perovskite crystal for efficient X-ray detection. Adv. Funct. Mater. **31**(21), 1–7 (2021). https://doi.org/10.1002/adfm.202100691
28. L. Mao, Y. Li, L. Yu, X. Li, J. Zhang, Stable and printable direct x-ray detectors based on micropyramid ω-Bi_2O_3 with low detection limit. IEEE Trans. Electron. Devices **68**(7), 3411–3416 (2021). https://doi.org/10.1109/TED.2021.3081528
29. B. Xin et al., Identifying carrier behavior in ultrathin indirect-bandgap $CsPbX_3$ nanocrystal films for use in UV/visible-blind high-energy detectors. Small **16**(43), 1–10 (2020). https://doi.org/10.1002/smll.202004513
30. P. Praveenkumar, T. Subashini, G.D. Venkatasubbu, T. Prakash, Crystallite size effect on low-dose X-ray sensing behaviour of Y_2O_3 nanocrystals. Sens. Actuators A **297**, 111544 (2019). https://doi.org/10.1016/j.sna.2019.111544